Available online at www.sciencedirect.com
SCIENCE DIRECT
Polymer 47 (2006) 2080–2090
polymer
www.elsevier.com/locate/polymer

Phase behaviour of a liquid crystalline polyetherester derived from 4′-hydroxy-1,1′-biphenyl-4-carboxylic acid and the ether-diol 4-(3-hydroxypropoxy)butan-1-ol

Aránzazu Martínez-Gómez *, Ernesto Pérez, Antonio Bello

Instituto de Ciencia y Tecnología de Polímeros (CSIC), Juan de la Cierva 3, 28006 Madrid, Spain

Received 22 December 2004; received in revised form 2 January 2006; accepted 11 January 2006

Abstract

The phase behaviour of PBO3O4, a liquid crystalline polyetherester derived from 4′-hydroxy-1,1′-biphenyl-4-carboxylic acid and the ether-diol 4-(3-hydroxypropoxy)butan-1-ol, has been investigated by differential scanning calorimetry (DSC), real-time synchrotron X-ray diffraction, optical microscopy and solid-state ^{13}C NMR. The results reveal an interesting polymesomorphism in PBO3O4, since, on cooling from the melt, a low-order smectic mesophase is obtained first, followed by a smooth transition into a slightly more ordered mesophase, and a final transition to a phase with a relatively high degree of order, stable at room temperature. The subsequent melting shows enantiotropic behaviour but, interestingly, the more ordered phase presents a considerably low undercooling. The ^{13}C NMR results in the solid-state of the ordered phase show that a single $T_{1\rho}^{H}$ relaxation time (and a single line shape for each particular carbon signal) is exhibited by PBO3O4. This fact, plus the low undercooling, suggests the formation of a highly ordered mesophase, instead of a three-dimensional crystal, which is the case of the corresponding polyester with the same spacer, or of the polyetherester with an all-methylene spacer. Additional experiments about the phase behaviour of the starting monomer for the synthesis of PBO3O4, reveal that a highly ordered mesophase is also obtained for the monomer, with a diffractogram rather similar to that exhibited by the ordered mesophase of the polymer.

Keywords: Liquid-crystalline polymers; Synchrotron X-ray analysis; Solid-state structure.

1. Introduction

Polyesters prepared by an alternating arrangement of biphenyl units as mesogenic groups and aliphatic spacers, $[PhPhCOOROOC]_n$, exhibit smectic mesophases and many works have been published concerning the influence of the nature of the spacer on the thermotropic behaviour of these polymers such as type of mesophases, thermal properties (transition temperatures and temperature range of stability of the mesophases) and crystallization rate [1–14]. Linear methylenic spacers ($R{=}(CH_2)_m$) with an even number of methylene units show SmA mesophases, while for odd spacers a SmCalt mesophase is found [1–4]. The odd–even nature of the spacer is also reflected in the temperatures and entropies of isotropization. Such an odd–even effect on thermodynamic parameters and mesophase structure has been explained as a consequence of the conformation of the spacer in the mesophase, which dictates the arrangement of the mesogenic cores in the smectic layer [15,16].

It has been proved that the thermal properties of the mesophases and their transformation rate can be controlled with suitable changes in the structure of the flexible spacer [7–14]. A factor that can be controlled is the stiffness of the molecular chains, governed by the number of conformations permitted to the system, which can be modified by inserting side groups and/or ether groups in the spacer. The information from previous works [7–10,16] indicates that as a result of substituting methylenic groups by ether linkages in the spacer, the thermal transitions of polyesters are shifted to lower temperatures, the thermodynamic behaviour becomes enantiotropic, and the rate of transformation of the mesophase into a more ordered phase is considerably decreased. Moreover, SmC phases have been reported for some oxymethylenic spacers [9,17] and methylenic spacers with methyl substitutents [12–14,18]. In recent works carried out in our laboratory, stable mesophases have been obtained using asymmetric

* Corresponding author. Address: E.T. S. de Ingenieros Industriales, Universidad Politécnica de Madrid, José Gutiérrez Abascal 2, 28006 Madrid, Spain.
E-mail address: arancham@etsii.upm.es (A. Martínez-Gómez).

0032-3861/$ - see front matter © 2006 Elsevier Ltd. All rights reserved.
doi:10.1016/j.polymer.2006.01.079

branched oxymethylenic spacers [10,19,20]. The odd–even effect on transition parameters and mesophase structure has been also found. It is evident, therefore, how important is the nature of the flexible spacer for the liquid crystalline behaviour of these polyesters.

Watanabe et al. [21] have studied the mesophase properties and structure of the main chain poly(etherester)s derived from 4′-hydroxybiphenyl-4-carboxylic acid and alkanediols, $[PhPhO(CH_2)_mOOC]_n$. These polymers contain two different linkage groups in the connection of the mesogen to the alkylene spacer: an ester group on one side and an ether group on the other. From information given in that study, it appears that the ether linkage produces similar odd–even effects than the ester linkage, although an opposite oscillation with *m* of the smectic structure is exhibited: for polymers with *m* even the mesophase is SmCalt and for polymers with *m* odd the mesophase is SmA. The observation of this opposite trend is due to the reduction by one unit of the segment that connects two successive biphenyl mesogens because of the lack of a carbonyl group in one of the two linkage groups.

No further studies on structural analyses have been made in relation to the odd–even character of flexible spacers in polyetheresters based on the biphenyl mesogen. On the other hand, little is known about the influence of the chemical nature of the spacer on their thermotropic properties because methylenic sequences have been the only spacers used at the moment.

In this paper, the synthesis and liquid crystalline behaviour of a polyetherester with oxymethylenic spacers derived from the ether-diol 4-(3-hydroxypropoxy)butan-1-ol, $HOCH_2CH_2$-$CH_2OCH_2CH_2CH_2CH_2OH$, are described. The ether-diol is even and, consequently, the polyetherester derived involves an odd spacer. The aim of this work is to establish the effect of the parity on the mesophase structure and also to investigate the influence of the presence of oxygen atoms in the spacer on the thermal properties. The investigated polyetherester is compared with its all-methylenic analogue (PHBC-8) [21] and with the polybibenzoate derived from the same ether-diol as spacer, whose synthesis and thermotropic properties were described in a previous work [17].

2. Experimental section

2.1. Synthesis

The polyetherester studied in this work was obtained according to Fig. 1.

2.1.1. Materials

The ether-diol 4-(3-hydroxypropoxy)butan-1-ol was synthesized as previously reported [17]. Ethyl 4′-hydroxy-1,1′-biphenyl-4-carboxylate and titanium (IV) isopropoxide, $(i\text{PrO})_4\text{Ti}$, from Aldrich Co. were used as received.

2.1.2. Synthesis of the monomers

The monomers for the synthesis of the polyetherester were obtained by reaction of ethyl 4′-hydroxy-1,1′-biphenyl-4-carboxylate with 4-(3-hydroxypropoxy)butan-1-ol under Mitsunobu conditions [22]. The detailed procedure for the synthesis is the following: triphenylphosphine (PPh_3) (2.35 g, 9 mmol), ethyl 4′-hydroxy-1,1′-biphenyl-4-carboxylate (2.17 g, 9 mmol) and 4-(3-hydroxypropoxy)butan-1-ol (2.65 g, 18 mmol) were dissolved in anhydrous tetrahydrofuran. The mixture was vigorously stirred and diethyl diazodicarboxilate (DEAD) (1.56 g, 9 mmol) was added dropwise at room temperature and the reaction mixture was left stirring overnight. The solvent was eliminated under vacuum and the solid residue was dissolved in dichloromethane. White needles of diethyl hydrazinedicarboxylate precipitated from the solution and were eliminated by filtration.

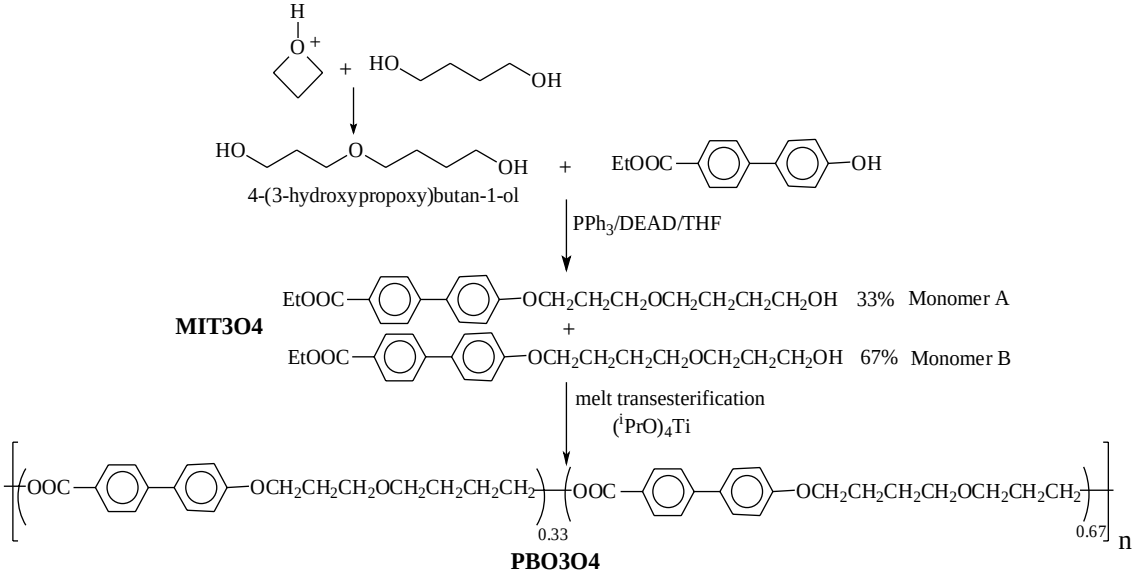

Fig. 1. Synthesis of polyetherester PBO3O4.

The filtrate was evaporated under vacuum and then purified by flash chromatography using silica gel with dichloromethane/ethyl acetate (7:3) as eluent. Yield 60%.

The diol 4-(3-hydroxypropoxy)butan-1-ol is asymmetrical and two different products of reaction: ethyl 4′-[3-(4-hydroxybutoxy)propoxy]-1,1′-biphenyl-4-carboxylate (monomer A) and ethyl 4′-[4-(3-hydroxypropoxy)butoxy]-1,1′-biphenyl-4-carboxylate (monomer B), that only differ in the position of the central ether of the aliphatic segment, can be formed (Fig. 1). Their polarities are similar and the separation by flash chromatography was not possible. This mixture of hydroxyester monomers, named MIT3O4, was used for the polymer synthesis.

The chemical structures of the monomers A and B were characterized by NMR spectroscopy in deuterated chloroform (^{1}H NMR spectrum is shown in Fig. 2). The proton and carbon peaks were assigned using COSY, HMQC and irradiation experiments. Irradiating at the resonance frequency of the quintuplet at 2.06 ppm, the ^{1}H NMR spectrum shows a singlet peak at 4.10 ppm instead of a triplet. This observation confirms the assignment of these signals to the protons Hb and Ha of monomer A. The composition of the mixture MIT3O4 can be determined from its ^{1}H NMR spectrum comparing the integrals of the signals associated with the protons Hh (δ = 4.37 ppm, $PhCOOC\mathbf{H}_2CH_3$, monomer A and monomer B) and Hb (δ = 2.06 ppm, $PhOCH_2C\mathbf{H}_2$, monomer A). The percentage of the monomers can also be calculated comparing the integrals of the triplets corresponding to the protons Ha (δ = 4.10 ppm, $PhOC\mathbf{H}_2$, monomer A) and Ha′ (δ = 4.00 ppm, $PhOC\mathbf{H}_2$, monomer B). The results show a proportion of 33 and 67% for monomer A and monomer B, respectively. The obtainment of such different percentages of monomers points out the different nucleophilic character of the hydroxylic groups in the asymmetric ether-diol 4-(3-hydroxypropoxy)butan-1-ol. This difference can be explained by a higher electron withdrawing effect of the ether when three methylene units separate the hydroxyl and the ether group.

^{1}H NMR ($CDCl_3$): δ = 1.39 (t, monomer A and monomer B, $PhCOOCH_2C\mathbf{H}_3$), 1.83 (m, monomer B, $PhOCH_2C\mathbf{H}_2C\mathbf{H}_2CH_2O$, monomer A, $OCH_2C\mathbf{H}_2C\mathbf{H}_2CH_2OH$), 2.06 (q, monomer A, $PhOCH_2C\mathbf{H}_2CH_2O$), 2.32 (t, monomer A, OH), 2.45 (t, monomer B, OH), 3.50 (m, monomer A, $OC\mathbf{H}_2CH_2CH_2CH_2OH$, monomer B, $PhOCH_2CH_2CH_2C\mathbf{H}_2O$), 3.62 (m, monomer A, $C\mathbf{H}_2OCH_2CH_2CH_2C\mathbf{H}_2OH$, monomer B, $OC\mathbf{H}_2CH_2CH_2OH$), 3.77 (c, monomer B, $OCH_2CH_2C\mathbf{H}_2OH$), 4.00 (t, monomer B, $PhOC\mathbf{H}_2$), 4.10 (t, monomer A, $PhOC\mathbf{H}_2$), 4.37 (c, monomer A and monomer B, $PhCOOC\mathbf{H}_2CH_3$), 6.95 (d, monomer A and monomer B, $C\mathbf{H}_{ar}CC$–O), 7.54 (d, monomer A and monomer B, $C\mathbf{H}_{ar}CH_{ar}CC$–O), 7.59 (d, monomer A and monomer B, $C\mathbf{H}_{ar}CH_{ar}CC$═O), 8.06 ppm (d, monomer A and monomer B, $C\mathbf{H}_{ar}CC$═O).

^{13}C NMR ($CDCl_3$): δ = 14.3 (monomer A and monomer B, $PhCOOCH_2\mathbf{C}H_3$), 26.0 (monomer B, $PhOCH_2\mathbf{C}H_2CH_2CH_2O$), 26.3 (monomer B, $PhOCH_2CH_2\mathbf{C}H_2CH_2O$), 26.7 (monomer A, $OCH_2\mathbf{C}H_2CH_2CH_2OH$), 29.6 (monomer A, $PhOCH_2\mathbf{C}H_2CH_2O$), 30.1 (monomer A, $OCH_2CH_2\mathbf{C}H_2CH_2OH$), 32.0 (monomer B, $OCH_2\mathbf{C}H_2CH_2OH$), 60.8 (monomer A and monomer B, $PhCOO\mathbf{C}H_2CH_3$), 62.1 (monomer B, $OCH_2CH_2\mathbf{C}H_2OH$), 62.7

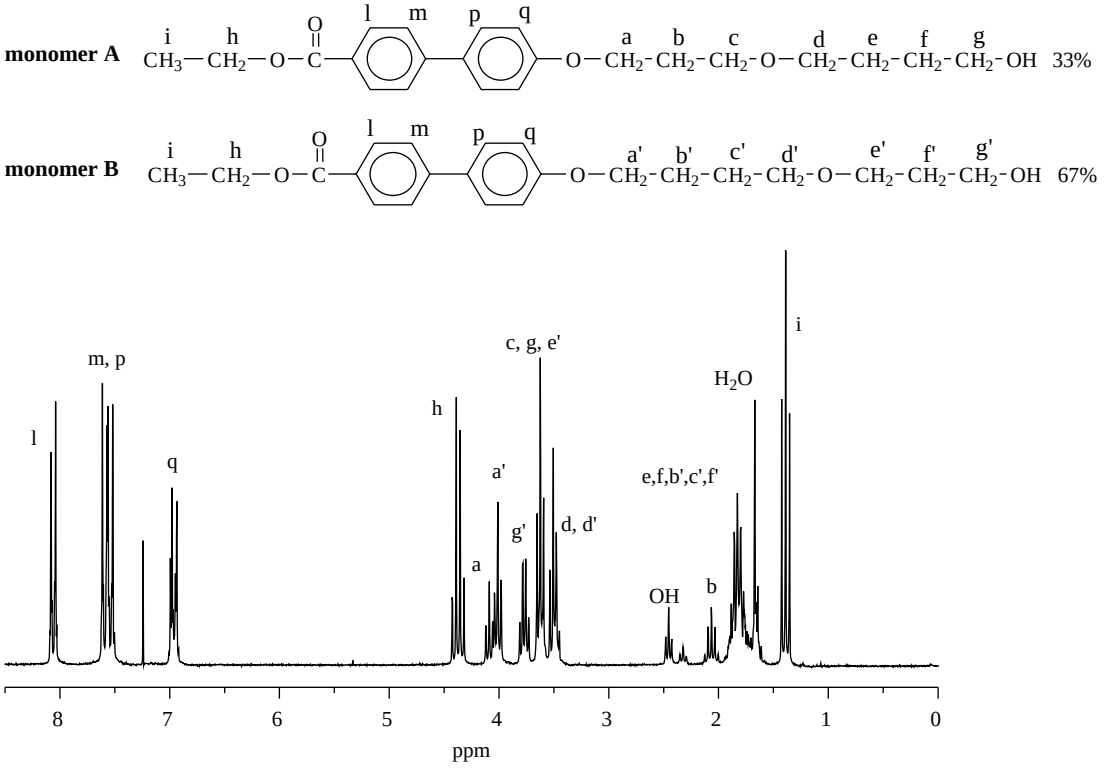

Fig. 2. ^{1}H NMR solution spectrum of MIT3O4.

(monomer A, $OCH_2CH_2CH_2\mathbf{C}H_2OH$), 64.9 (monomer A, $PhO\mathbf{C}H_2$) 67.3 (monomer A, $PhOCH_2CH_2\mathbf{C}H_2O$), 67.7 (monomer B, $PhO\mathbf{C}H_2$), 70.1 (monomer B, $O\mathbf{C}H_2CH_2CH_2OH$), 70.8 (monomer B, $PhOCH_2CH_2CH_2\mathbf{C}H_2O$), 71.0 (monomer A, $O\mathbf{C}H_2CH_2CH_2CH_2OH$), 114.9 (monomer A and monomer B, $\mathbf{C}H_{ar}C$–O), 126.3 (monomer A and monomer B, $\mathbf{C}H_{ar}CH_{ar}$-CC=O), 128.3 (monomer A and monomer B, $\mathbf{C}H_{ar}CH_{ar}C$–O), 128.4 (monomer A and monomer B, $\mathbf{C}CH_{ar}CH_{ar}C$–O), 128.5 (monomer A and monomer B, $CH_{ar}\mathbf{C}C$=O), 130.0 (monomer A and monomer B, $\mathbf{C}H_{ar}CC$=O), 145.1 (monomer A and monomer B, $\mathbf{C}CH_{ar}CH_{ar}CC$=O), 159.2 (monomer A and monomer B, $CH_{ar}\mathbf{C}$–O), 166.5 ppm (monomer A and monomer B, $\mathbf{C}$=O).

A 15% fraction of the dicondensed product ethyl 4′-[3-(4-{[4′-(ethoxycarbonyl)-1,1′-biphenyl-4-yl]oxy}butoxy)propoxy]-1,1′-biphenyl-4-carboxylate was also obtained. This fraction was easily removed from the monomer by flash chromatography under the conditions mentioned above.

2.1.3. Synthesis of the polymer

The polyetherester, named as PBO3O4, was synthesized by melt transesterification of the mixture MIT3O4 (monomer A (33%) and monomer B (67%)). The catalyst, $(i\mathrm{PrO})_4$Ti, was added to the melted monomers and the reaction mixture was heated at 200 °C under a N_2 atmosphere for 3 h. In a second step, polycondensation was carried out at higher temperature (220–250 °C) under reduced pressure (0.01 mm Hg) for 4 h. The polymer was purified by dissolving in hot chloroform and precipitating in excess methanol. The polymer was collected by filtration, washed with methanol and dried in vacuum. The recovered material was close to 90% of the theoretical yield.

The chemical structure of the polymer was characterized by NMR spectroscopy in deuterated chloroform. The ^{1}H NMR and ^{13}C NMR signals (Fig. 3) were assigned using COSY and HMQC experiments. The spectra do not show any unexpected signals. The polymer composition can be determined from its ^{1}H NMR spectrum by comparison of the integrals of the triplets assigned to the protons Ha (δ=4.10 ppm, $PhOC\mathbf{H}_2$, monomer A) and Ha′ (δ=4.00 ppm, $PhOC\mathbf{H}_2$, monomer B) or comparing the signals of Hg (δ=4.33 ppm, $PhCOOC\mathbf{H}_2$, monomer A) and Hg′ (δ=4.42 ppm, $PhCOOC\mathbf{H}_2$, monomer B). It was found that the ratio of the two monomers in the polymer backbone corresponds very well with the composition of the monomer mixture MIT3O4 used in the polymerization reaction.

2.2. Techniques

The thermal behaviour of the polymer and of the monomer was studied by differential scanning calorimetry (DSC) experiments. DSC measurements were carried out with a Perkin–Elmer DSC7 calorimeter, provided with a cooling system.

The phase transitions and the nature of the phases involved were investigated by real-time X-ray diffraction experiments with synchrotron radiation. The short acquisition times required for the synchrotron experiments make this technique

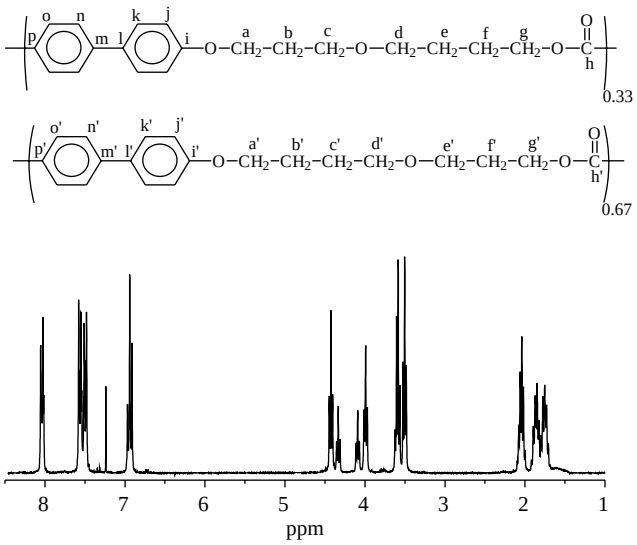

^{1}H-NMR (CDCl $_3$, 40 °C): δ = 1.75 (m, 4H, He and Hc'), 1.85 (m, 4H, Hf and Hb'), 2.04 (m, 4H, Hb and Hf'), 3.50 (t, 4H, Hd and Hd'), 3.58 (t, 2H, He'), 3.60 (t, 2H, Hc), 4.00 (t, 2H, Ha'), 4.10 (t, 2H, Ha), 4.33 (t, 2H, Hg), 4.42 (t, 2H, Hg'), 6.94 (m, 4H, Hj and Hj'), 7.53 (m, 8H, Cn, Cn', Ck and Ck'), 8.04 (m, 4H, Co and Co') ppm.

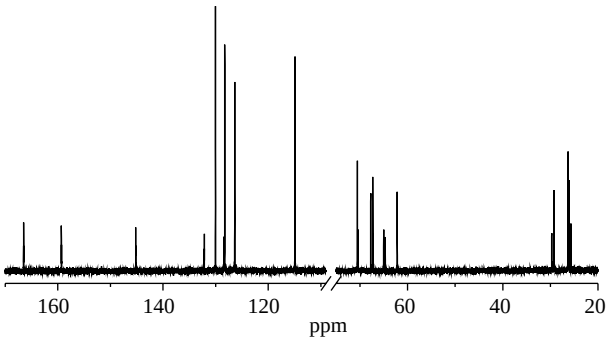

^{13}C-NMR (CDCl $_3$, 40 °C): δ = 25.7 (Cf), 26.1 (Cb'), 26.3 (Ce and Cc'), 29 .4 (Cf'), 29.7 (Cb), 62.2 (Cg'), 64.7 (Cg), 65.0 (Ca), 67.2 (Cc), 67.3 (Ce'), 67.7 (Ca'), 70.4 (Cd), 70.5 (Cd'), 114.9 (Cj and Cj'), 126.4 (Cn and Cn'), 128.3 (Ck and Ck'), 128.4 (Cl and Cl'), 130.0 (Co and Co'), 132.2 (Cp and Cp'), 145.2 (Cm and Cm'), 159.3 (Ci and Ci'), 166.5 (Ch and Ch') ppm.

Fig. 3. ^{1}H NMR and ^{13}C NMR solution spectra of PBO3O4.

particularly useful for the characterization of liquid crystal systems where more than one mesophase are formed, or where the mesophases present a short interval of existence. These experiments were performed at the polymer beamline at Hasylab (Desy, Hamburg). The beam was monochromatized (λ=0.150 nm) by Bragg reflection through a germanium single crystal. Two linear position-sensitive detectors were used simultaneously, one of them fixed and covering the approximate 2θ range from 10 to 30°, and the other being set at two different sample-detector positions (in the direction of the beam): 43 and 190 cm, respectively. The first position covers the approximate 2θ range from 1.1 to 8.8° (spacings from 8 to 1 nm), and the second, from about 0.24 to 2.70° (spacings from about 35 to 3.2 nm). Therefore, wide-angle (WAXS), middle-angle (MAXS) and small-angle (SAXS) scattering data are

collected in the two experimental set-ups: simultaneous WAXS/MAXS profiles are acquired in the first case, and WAXS/SAXS in the second.

Film samples, of about 20 mg, were covered by aluminum foil, in order to ensure homogeneous heating or cooling, and placed in the temperature controller of the beamline, under vacuum. Heating or cooling experiments were performed at a rate of 8 °C/min. The same temperature program was reproduced in the two set-ups, and the WAXS data were used to monitor the reproducibility of the results. The reproducibility was found to be well inside the inherent experimental resolution of the system.

The scattering patterns were collected in time frames of 30 or 15 s, so that we have a temperature resolution of 4 or 2 °C between frames. The calibration of the spacings for the different detectors and positions was made as follows: the diffractions of a crystalline PET sample were used for the WAXS detector; a sample of silver behenate (giving a well-defined diffraction at a spacing of 5.838 nm, and several orders) was used for the MAXS detector; and the different orders of the long spacing of rat-tail cornea ($L=65$ nm) for the SAXS detector.

Fiber patterns were also obtained, at room temperature, in the same synchrotron beamline but with a different configuration: an image plate detector, located at 20.5 cm from the sample, was used for the WAXS/MAXS region, and a CCD detector, at 307 cm from the sample, for the SAXS region.

The polymer film for DSC and synchrotron measurements was prepared by molding the material in a Collin press above the melting temperature and then cooled to room temperature.

The mesophase textures were studied using a Carl Zeiss polarizing microscope equipped with a Linkam TMS92 hot stage.

Solid-state ^{13}C NMR spectra were acquired, at room temperature, on a Bruker AVANCE 400 spectrometer, operating at 100.615 MHz. The sample, inside 4-mm rotors, was rotated at 7000 Hz. A cross-polarization, CP, time of 1 ms was used, with different spin-locking, SL, times. Typically, 5000 transients were acquired for each experiment, using a recycle delay of 5 s. A secondary standard, adamantane, was employed as reference for the chemical shift.

3. Results and discussion

The DSC cooling and heating curves at 8 °C/min of PBO3O4 are shown in the lower part of Fig. 4. Three exotherms at 179 °C ($\Delta H=11.3$ J/g), 166 °C ($\Delta H=9.1$ J/g) and 122 °C ($\Delta H=9.6$ J/g) are obtained on cooling from the isotropic melt. In the subsequent heating cycle, three endotherms at 128 °C ($\Delta H=9.9$ J/g), 191 and 194 °C appear. The two endotherms at higher temperature are overlapped, and the total enthalpic change is 20.8 J/g.

Three exotherms were also observed for the polybibenzoate with the same spacer [17]. In that case, the lower temperature one was attributed to the formation of a three-dimensional crystal structure, while the other two involved low-ordered mesophases (SmA and SmC). In the present case, the lower

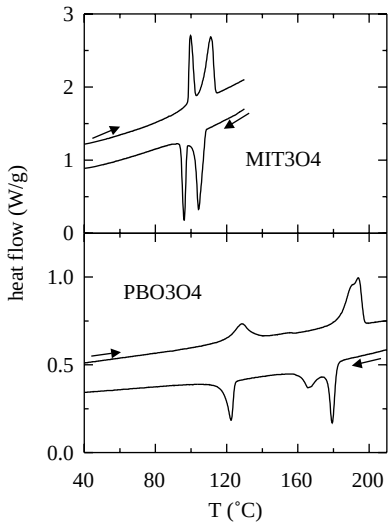

Fig. 4. DSC curves of monomer MIT3O4 (upper) and of the polymer PBO3O4 (lower) corresponding to the cooling from the isotropic melt and the subsequent heating. Scanning rate: 8 °C min^{-1}.

temperature phase might be also attributed to a crystal structure. However, there is a clear difference between the two polymers: the crystal phase of the polyester presents a considerably high undercooling, while in the polyetherester the undercooling for the low-temperature phase is rather small: of the order of only 6 °C, as observed in Fig. 4 (for the actual scanning rate of 8 °C/min). This low undercooling is not usual when crystalline phases are involved.

The MAXS/WAXS synchrotron profiles obtained for PBO3O4 during a cooling cycle at 8 °C/min are presented in Fig. 5 and the results obtained in the analysis of the diffractograms are displayed in Figs. 6 and 7. It can be observed that, at temperatures between 216 and 180 °C the diffractograms show only a broad halo in the WAXS region, centred at 0.48 nm, corresponding to the averaged intermolecular

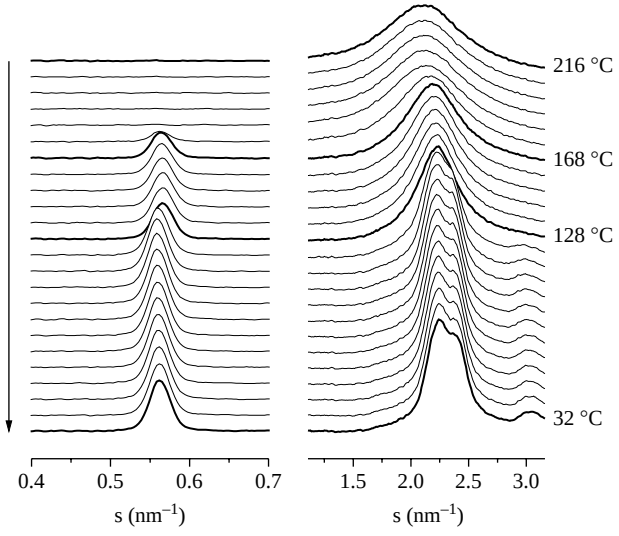

Fig. 5. X-ray diffraction patterns in the MAXS (left side) and WAXS (right side) regions of PBO3O4 recorded at an experimental rate of 8 °C min^{-1} during the cooling from the isotropic melt. For clarity, only one of every two frames is plotted.

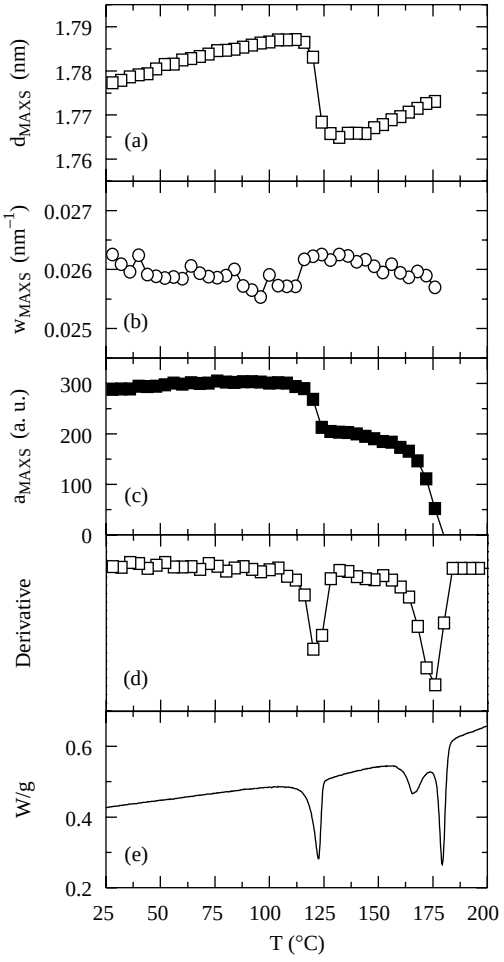

Fig. 6. Variation of the position of the MAXS peak (a), width (b), total area (c) and derivative of the area (d) as a function of temperature corresponding to PBO3O4 in the cooling experiment, at 8 °C min^{-1}, of Fig. 5. The DSC cooling curve, at 8 °C min^{-1}, (e) is also presented for comparison.

distances in the isotropic melt. On lowering the temperature, at 176 °C a MAXS peak appears at around 1.773 nm (s = 0.564 nm^{-1}). At the same time, a narrowing and a slight change in the position of the WAXS halo are observed (see diffractogram at 168 °C in Fig. 5). These observations indicate the formation of a smectic phase with disordered layers. A further decrease in temperature produces the following changes in the diffractograms. First, the intensity of the amorphous-like halo (now placed at around 0.46 nm) increases and the halo becomes sharper while the MAXS peak changes its position very slightly (see diffractogram at 128 °C in Fig. 5 and results displayed in Fig. 6). All this seems to indicate that a mesophase with a slightly higher degree of order is obtained, most probably a SmB mesophase with a rather disordered hexagonal packing within the smectic layers.

On further cooling, the WAXS region starts to show remarkable changes when the temperature approaches 124 °C: three diffraction peaks appear at 0.454, 0.420 and 0.336 nm, respectively. Moreover, the MAXS diffraction shifts from around 1.765 nm just before the transition to 1.787 nm after the transition. We are dealing, therefore, with a phase of a considerable degree of order. This phase is stable at room

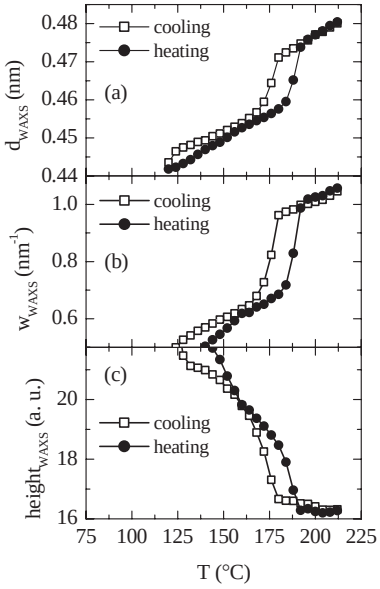

Fig. 7. Variation of the position (a) width (b) and height (c) of the WAXS broad peak as a function of temperature for PBO3O4, for both the cooling and the heating experiments.

temperature, where the spacings for the WAXS peaks are 0.448, 0.415 and 0.328 nm (s values of 2.230, 2.410 and 3.042 nm^{-1}, respectively), while the MAXS peak is now centred at 1.777 nm (s = 0.563 nm^{-1}).

All the phases formed by PBO3O4 show smectic spacings close to the length of the extended repeating unit (L = 2.10 nm). Moreover, no variation with temperature of these spacings, besides the effect of thermal contraction, has been detected in the synchrotron X-ray diffraction experiments, so it can be considered that the phases formed by PBO3O4 seem to be orthogonal structures. In the case of the polyester with the same spacer, a tilted SmC mesophase is obtained, when lowering the temperature, from the initial orthogonal SmA phase.

Mechanically aligned samples were made in order to obtain X-ray patterns at room temperature of the oriented polymer that permit us to confirm this orthogonal structure. We failed to quench the low-ordered mesophases, so that only the diffraction pattern of the more ordered phase could be obtained. This pattern is presented in Fig. 8, and shows two sharp inner reflections, located at 1.770 and 0.885 nm, attributed to the layer spacing and its second order. They appear on the meridian, indicating that the normal direction of the layers is parallel to the fiber (macromolecular direction). Therefore, and considering the small changes in the layer spacing on passing through the different transitions, it can be concluded that the phases of PBO3O4 are upright structures.

The detailed analysis of the MAXS/WAXS experiments on cooling PBO3O4 from the isotropic melt is presented in Figs. 6 and 7. As mentioned above, the MAXS peak appears at around 176 °C, coinciding with the first exotherm observed in the DSC cooling curve, and a clear increase in the MAXS spacing is detected (Fig. 6(a)) centred at around 122 °C (third exotherm).

The width of the MAXS peak presents only a slight decrease at around 120 °C (Fig. 6(b)). However, no noticeable change in

Fig. 8. Image plate X-ray photograph of a PBO3O4 fibre, acquired at room temperature. Stretching direction vertical.

the position, or in the width of the MAXS peak is observed at temperatures around 166 °C, where the second DSC exotherm is obtained.

The variation with temperature of the area of the MAXS peak is presented in Fig. 6(c), showing again only two clear changes, centred at 176 and 122 °C, as observed more clearly in its derivative (Fig. 6(d)). The comparison of this derivative with the DSC cooling curve (Fig. 6(e)) indicates that, although there is a general rather good coincidence between the synchrotron and DSC results, however, the two transitions at higher temperatures observed in the DSC cooling curve are not resolved in the MAXS results.

The WAXS results are presented in Fig. 7, showing the variation of the position, width and height of the amorphous-like halo (before the obtainment of the final low-temperature phase, which shows clear diffraction peaks). Again, only a clear change of both magnitudes is observed at around 176 °C, while no discontinuity is observed at lower temperatures. However, as observed in Fig. 5, the amorphous-like halo experiences a rather noticeable decrease in width and increase in its maximum intensity between the formation of the initial low-ordered mesophase and the final low-temperature more ordered phase. That decrease in the width and increase in the height appears to be much higher than the ones found when only low-ordered mesophases, like SmA or SmC, are involved [17,23,24].

A phase behaviour rather similar to the one exhibited by PBO3O4 has been reported for liquid crystalline polyoxetanes [23] with side chains including two biphenyl mesogens also connected by ether and ester linkages to different flexible spacers and terminal segments. These side-chain polyoxetanes exhibit much more clearly the intermediate formation of a disordered hexagonal SmB mesophase, and the single WAXS peak obtained for that mesophase is considerably narrower than the one obtained here for PBO3O4. Thus, a width of only around 0.2 nm^{-1} is reported for one of those polyoxetanes, indicating a higher degree of order inside the smectic layers. However, it has to be taken into account that the considerably higher side-chain mobility may be responsible of obtaining a higher order.

From all these previous results, and considering that all the phases involved seem to be orthogonal, a probable explanation is that a low-ordered SmA or SmCalt mesophase is formed first on cooling from the melt, and such phase experiences a rather smooth change into a slightly more ordered mesophase: most probably a SmB mesophase. Regarding the final ordered phase, we will come to its nature later on.

The MAXS/WAXS diffraction patterns corresponding to the subsequent melting experiment are presented in Fig. 9. A phase sequence opposite to that obtained on cooling is observed, revealing the enantiotropic behaviour of PBO3O4. Moreover, the detailed analysis of the diffractograms leads to rather similar results to those obtained on cooling. For instance, the variation of the position, width and area of the MAXS peak is practically the same as that presented in Fig. 6 for the cooling experiment, with the only difference of the small temperature shift of the two clear 'transitions', which on heating appear centred at 132 and 188 °C. Regarding the WAXS results for the amorphous-like halo, the variation of its position and width is presented in Fig. 7, compared with the cooling results, and showing the commented parallelism.

Additional SAXS/WAXS experiments have been performed on PBO3O4. The SAXS profiles corresponding to a melting experiment are presented in Fig. 10. No long spacing is detected at any temperature, contrary to the case of other similar liquid-crystalline polymers where crystalline phases are involved [17,25,26]. Of course, it may happen that the long spacing falls outside the detector's window, or there is not enough electron density differences among the sample (no long spacing was detected neither in the fiber SAXS pattern obtained in the CCD detector, which, for the actual configuration, presents a lower limit for the detector's windows of around 66 nm). But considering the results in other polymers and the fact of the very low undercooling exhibited

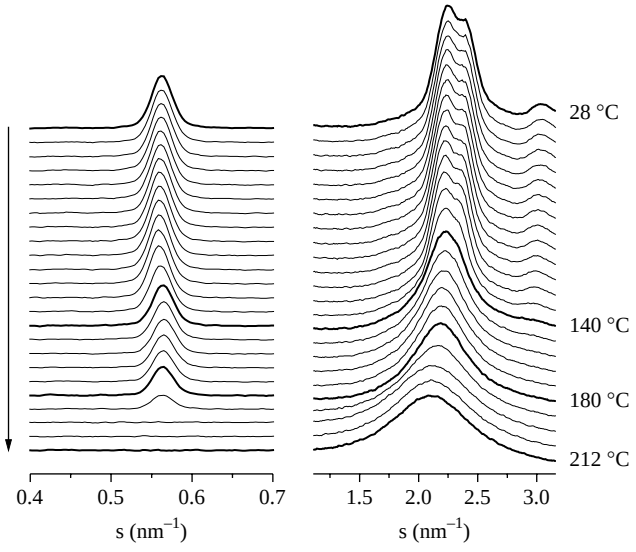

Fig. 9. X-ray diffraction patterns in the MAXS (left side) and WAXS (right side) regions of PBO3O4 recorded at an experimental rate of 8 °C min^{-1} during the heating. For clarity, only one of every two frames is plotted.

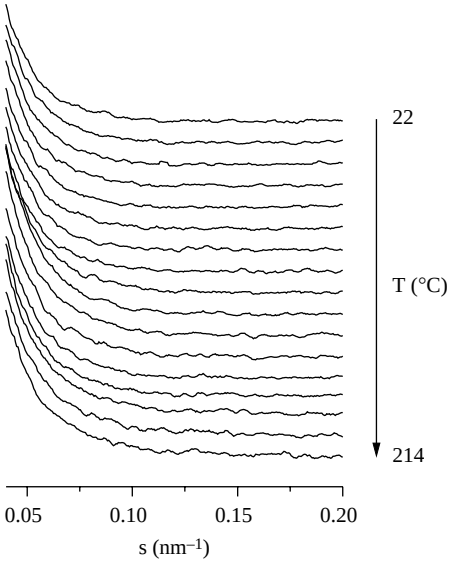

Fig. 10. SAXS profiles of PBO3O4 in a heating experiment at 4 °C min^{-1}. For clarity, only one of every three frames is plotted.

by the low-temperature phase, it seems that we are dealing with a highly ordered mesophase and not with a three-dimensional crystal. From the previous diffraction results, such phase is orthogonal, so that it is most probably a smectic crystal of the type SE: a smectic crystal with orthorhombic structure and orthogonal alignment of the chains, but with rotational disorder that differentiates it from a truly three-dimensional crystal.

A close inspection of the SAXS profiles in Fig. 10 reveals that there are subtle changes at the known transitions. In fact, Fig. 11 presents the variation of the relative SAXS invariant [27–29] showing small but clear increases at the two transition regions, indicating, most probably, some differences in the density fluctuations among the different phases.

In order to get a further insight about the nature of the ordered phase, several solid-state ^{13}C NMR experiments were performed on a sample of PBO3O4, acquired with CP-MAS techniques, and with variable spin-locking (SL) times. Fig. 12 shows the spectrum corresponding to a 0.01 ms SL time

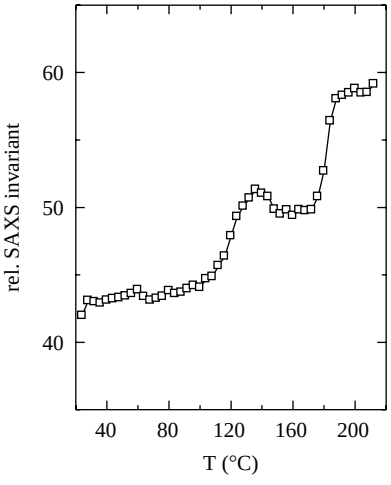

Fig. 11. Temperature dependence of the relative SAXS invariant corresponding to the melting experiment in Fig. 10.

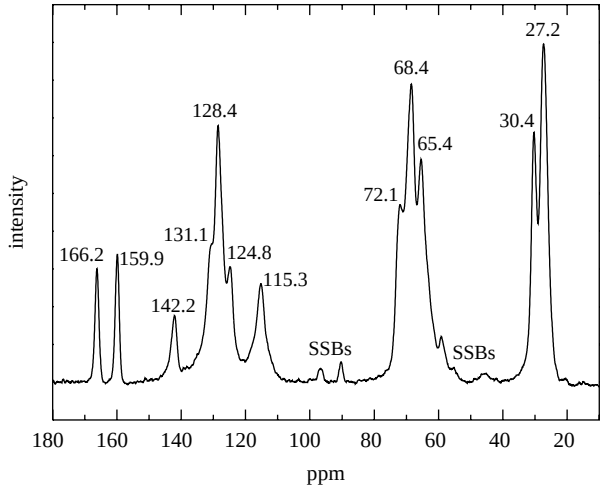

Fig. 12. Solid-state ^{13}C CP-MAS experiment, at room temperature, for PBO3O4, acquired with a SL time of 0.01 ms.

(a negligible time). The chemical shifts for the different resolvable resonances are indicated. They correspond very well with the solution chemical shifts shown in Fig. 3. Fig. 13 shows the amplification of the aliphatic carbons region for the spectra acquired with 0.01 and 4 ms SL time (this last one amplified by a factor of 2.96). The spectrum with the negligible SL time will be representative of the possible different phases present in the sample, even though the relative proportions may be somewhat distorted, owing to possible differences in CP efficiency. On the other hand, the spectrum with 4 ms SL time, besides the decrease in peak intensities by a factor of 2.96, shows exactly the same line shapes than the one with the 0.01 SL time, indicating that $T_{1\rho}^{H}$ is quite uniform throughout the sample. Moreover, the decay of the magnetization with the SL time is plotted in Fig. 14. A perfect straight line is followed, corresponding to a single $T_{1\rho}^{H}$ of 3.6 ms. The most probable interpretation of these uniformities is that a single phase is present, i.e. a highly ordered mesophase that occupies practically 100% of the whole sample, contrary to the case of

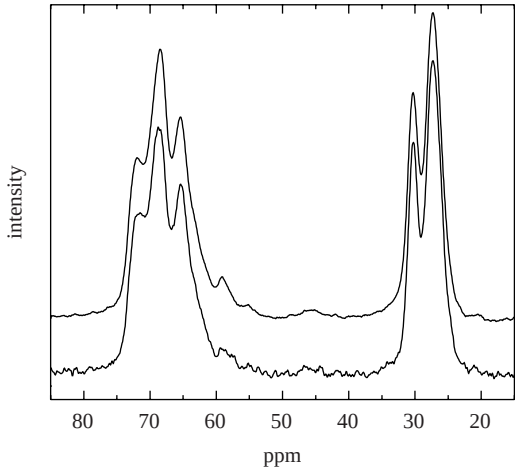

Fig. 13. Solid-state ^{13}C CP-MAS spectra, showing the aliphatic region, corresponding to PBO3O4 acquired with 0.01 ms (upper) and 4 ms (lower) SL times. The lower spectrum has been multiplied by a factor of 2.96.

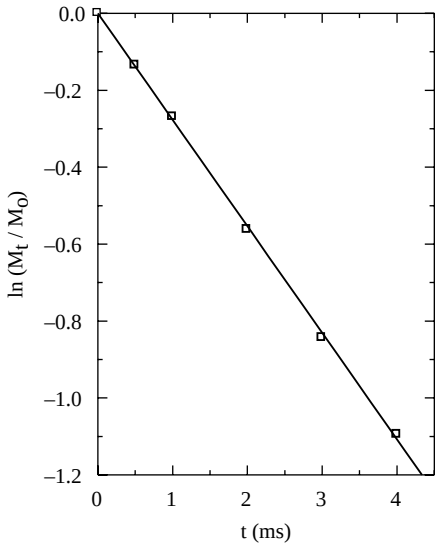

Fig. 14. Evolution of the magnetization with the spin-locking time for a PBO3O4 sample in CP-MAS experiments with variable spin locking time.

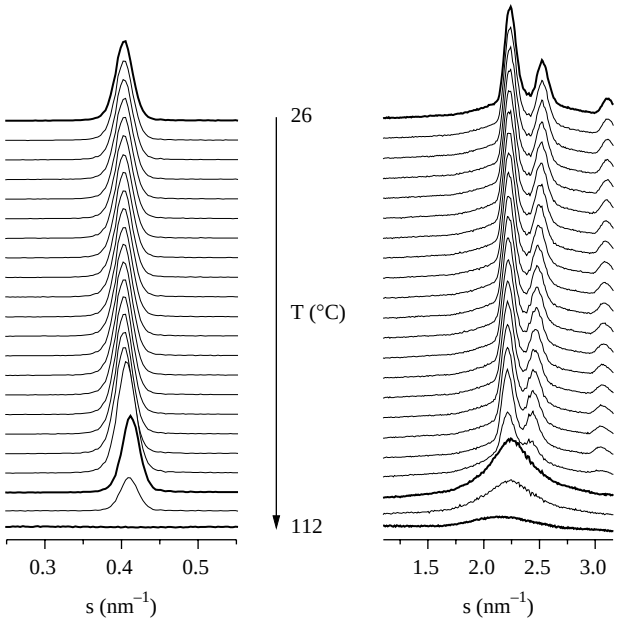

Fig. 15. X-ray diffraction patterns in the MAXS (left side) and WAXS (right side) regions of MIT3O4 recorded every 15 s during the heating at 8 °C min^{-1}. For clarity, only one of every two frames is plotted.

the crystalline phases found in other similar systems, where semicrystalline samples are reported [26,30] with two well different $T_{1\rho}^{H}$ values. In fact, preliminary results on a sample of the polyester with the same spacer, indicate also the presence of two phases with different $T_{1\rho}^{H}$ values (and line shapes), as correspond to a semicrystalline sample [17].

Attempts were also made in order to identify, by optical microscopy, the textures corresponding to the different phases. Unfortunately, and as it happens with LC polymers of high or relatively high-molecular weights, no identifiable textures were obtained.

For that reason, we decided to perform a complementary study of the phase behaviour corresponding to the starting monomer, named as MIT3O4. DSC, optical microscopy and X-ray diffraction experiments indicate that MIT3O4 exhibits liquid crystalline properties. It presents two thermal transitions with small undercooling. Thus, the upper part of Fig. 4 shows that, on cooling from the melt, two exotherms are obtained, at 104 °C (with an enthalpy of 22.9 J/g) and 94 °C (enthalpy of 13.0 J/g), while on heating the two endotherms appear at 100 °C (13.4 J/g) and 111 °C (22.5 J/g).

The first transition observed on cooling from the isotropic melt corresponds to the formation of a smectic mesophase with disordered layers, since the diffractogram obtained for this phase presents a MAXS peak at 2.42 nm ($s=0.413$ nm^{-1}), due to the regular piling of smectic layers, and a broad halo at 0.445 nm ($s=2.247$ nm^{-1}) in the WAXS region, corresponding to the disordered lateral arrangement of the molecules within the layers. In the second transition the smectic mesophase is transformed into a phase of more symmetry which shows three reflections in the WAXS region (0.446, 0.397 and 0.321 nm) and a smectic spacing at 2.47 nm ($s=0.405$ nm^{-1}).

A reverse phase behaviour is observed on melting (Fig. 15): the ordered phase is transformed into the low-ordered mesophase at around 100 °C, and this melts at around 110 °C, in perfect agreement with the DSC results.

At this point it is interesting to consider the low enthalpy involved in the formation of the low-temperature phase, and that only one order is observed for the MAXS spacing. These two facts are not supporting the formation of a crystalline phase, and a highly ordered mesophase is more probable.

Fig. 16 shows the revealing birefringence textures observed with an optical microscope. At room temperature MIT3O4 shows a focal-conic fan texture over a mosaic texture (see photograph a). Moreover, the presence of coloured concentric arcs in the smectic fans is observed. The striated fan-shaped texture and mosaic texture are commonly developed by highly ordered smectic phases [31]. Increasing the temperature, and coinciding with the first thermal transition in the DSC heating curve, the concentric arcs of the fans disappear at the same time that the mosaic texture vanishes, and a simple focal-conic texture, corresponding to a low-order smectic mesophase is then observed (see photograph b). As diffraction experiments showed, the second thermal transition corresponds to the isotropization of the mesophase: the focal-conic texture vanishes and the isotropic melt is observed in the microscope.

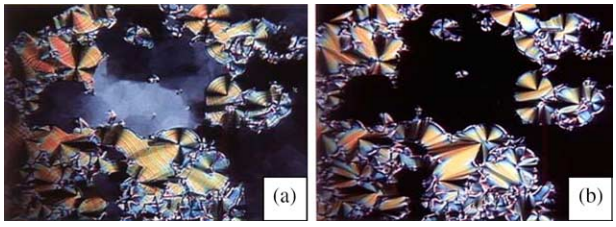

Fig. 16. Representative optical polarized micrographs of MIT3O4. (a) Texture observed at room temperature after cooling from the isotropic melt. (b) Focal-conic texture of the S_A mesophase at 108 °C upon heating.

Table 1
Phase sequence exhibited by the polyetherester PBO3O4 compared to those of P3O4B, the polyester with the same spacer, and PHBC-8, the polyetherester with the corresponding all-methylene spacer

Polymer	Phase sequence[a]
PHBC-8[21]	I 193 SmCalt 147 Cr
PBO3O4	I 179 SmA or SmCalt 166 SmB 122 SE
P3O4B[17]	I 147 SmA–SmC 52 Cr

[a] On cooling from the isotropic melt. The numbers indicate the transition temperatures in °C.

As commented above, the two phases observed show layer periodicities of 2.42 and 2.47 nm, respectively, very close to the fully extended length of the molecule ($L=2.50$ nm). This suggests the presence of orthogonal phases. Considering, therefore, all the previous results, the phase sequence obtained for MIT3O4 on cooling is, probably, the following: isotropic melt, low-ordered SmA mesophase and highly ordered SE smectic crystal.

In fact, the three WAXS reflections observed in Fig. 15 can be tentatively assigned to the (110), (200) and (210) planes of an orthorhombic packing with $a=0.794$ nm, $b=0.539$ nm and $c=2.47$ nm.

It can be concluded, therefore, that the monomer MIT3O4 presents a phase behaviour rather similar to that of the polymer PBO3O4, with the exception of the considerably lower transition temperatures in the monomer (as expected), and the fact that only one low-ordered mesophase is observed in the monomer (probably due to the smaller temperature interval between the transitions).

This similarity reinforces the assignment of the ordered phase of the polymer to a SE smectic crystal, most probably, with an orthorhombic packing. In fact, and similarly to the monomer, the three WAXS diffractions of the polymer (see above) can be assigned to the (110), (200) and (210) planes of an orthorhombic packing with $a=0.830$ nm, $b=0.523$ nm and $c=1.78$ nm.

Finally, Table 1 shows the comparison of the phase sequences exhibited by the polyetherester PBO3O4, the polyester with the same spacer, P3O4B, and PHBC-8, the polyetherester with the corresponding all-methylene spacer. It can be observed, first, that the transition temperatures exhibited by PBO3O4 are intermediate between those of the other two polymers. This is a expected result since PHBC-8 with an all-methylene, less flexible spacer than that for PBO3O4, shall present the highest transition temperatures, while the polyester P3O4B, prepared with the same diol than PBO3O4, includes an extra carbonyl group in the spacer, i.e. its length is higher.

But the most interesting feature from the inspection of the phase sequences in Table 1 is the fact that the inclusion of oxygen atoms in the spacer leads to an extended polymesomorphism, since more than one type of mesophases are observed: two in the case of P3O4B and three in the present case of PBO3O4. Therefore, very simple changes in the spacer (and/or in the connecting groups) lead to a rather different phase behaviour.

4. Conclusions

In conclusion, the results reveal an interesting polymesomorphism in PBO3O4, since, on cooling from the melt, a low-order SmA or SmCalt mesophase is obtained first, followed by a smooth transition into a slightly more ordered SmB mesophase, and a final transition to a phase with a relatively high degree of order, stable at room temperature, assigned as a smectic crystal SE. The subsequent melting shows enantiotropic behaviour but, interestingly, the more ordered phase presents a considerably low undercooling.

The ^{13}C NMR results in the solid state of the ordered phase show that a single $T_{1\rho}^{H}$ relaxation time (and a single line shape for each particular carbon signal) is exhibited by PBO3O4. This fact, plus the low undercooling, suggests the formation of a highly ordered mesophase, instead of a three-dimensional crystal, which is the case of the corresponding polyester with the same spacer, or of the polyetherester with an all-methylene spacer.

Additional experiments about the phase behaviour of the starting monomer for the synthesis of PBO3O4, reveal that a highly ordered mesophase (most probably a smectic crystal of the SE type) is also obtained for the monomer, with a diffractogram rather similar to that exhibited by the ordered mesophase of the polymer.

Acknowledgements

We acknowledge the financial support of MEC, Project No MAT2004-06999-C02-01 and Project No MAT2004-06999-C02-02. The synchrotron work was supported by the European Community—Research Infrastructure Action under the FP6 'Structuring the European Research Area' Programme (through the Integrated Infrastructure Initiative 'Integrating Activity on Synchrotron and Free Electron Laser Science'), contract RII3-CT-2004-506008 (IA-SFS). We thank the collaboration of the Hasylab personnel.

References

[1] Pérez E, Pereña JM, Benavente R, Bello A. In: Cheremisinoff NP, editor. Handbook of engineering polymeric materials. New York: Marcel Dekker; 1997. p. 383–97.
[2] Watanabe J, Hayashi M, Nakata Y, Niori T, Tokita M. Prog Polym Sci 1997;22:1053.
[3] Watanabe J, Hayashi M. Macromolecules 1988;21:278.
[4] Watanabe J, Hayashi M. Macromolecules 1989;22:4083.
[5] Meurisse P, Nöel C, Monnerie L, Fayolle B. Br Polym J 1981;13:55.
[6] Krigbaum WR, Asrar J, Toriumi H, Ciferri A, Preston J. J Polym Sci, Polym Lett Ed 1982;20:109.
[7] Bello A, Pereña JM, Pérez E, Benavente R. Macromol Symp 1994; 84:297.
[8] Bello A, Pérez E, Marugán MM, Pereña JM. Macromolecules 1990; 23:905.
[9] Pérez E, Riande E, Bello A, Benavente R, Pereña JM. Macromolecules 1992;25:605.
[10] Bello P, Bello A, Riande E, Heaton NJ. Macromolecules 2001;34:181.
[11] Loman AJB, Van Der Does E, Bantjes A, Vulic I. J Polym Sci, Part A: Polym Chem 1995;33:493.
[12] Watanabe J, Hayashi M, Kinoshita S, Niori T. Polym J 1992;24:597.

[13] Del Campo A, Pérez E, Bello A, Benavente R, Pereña JM. Polymer 1998; 39:3847.
[14] Pérez E, Del Campo A, Bello A, Benavente R. Macromolecules 2000; 33:3023.
[15] Abe A. Macromolecules 1984;17:2280.
[16] Bello A, Riande E, Pérez E, Marugán MM, Pereña JM. Macromolecules 1993;26:1072.
[17] Martínez-Gómez A, Bello A, Pérez E. Macromolecules 2004;37:8634.
[18] Watanabe J, Hayashi M, Motita A, Tokita M. Macromolecules 1995; 28:8073.
[19] Martínez-Gómez A, Pereña JM, Lorenzo V, Bello A, Pérez E. Macromolecules 2003;36:5798.
[20] Martínez-Gómez A, Bello A, Pérez E. Eur Polym J, Submitted for pulication.
[21] Nakata Y, Watanabe J. J Mater Chem 1994;4:1699.
[22] Mitsunobu O. Synthesis 1981;1.
[23] Martínez-Gómez A, Bello A, Pérez E. Macromol Chem Phys 2005; 206:1731.
[24] Pérez E, Benavente R, Cerrada ML, Bello A, Pereña JM. Macromol Chem Phys 2003;204:2155.
[25] Todorova G, Krasteva M, Pérez E, Pereña JM, Bello A. Macromolecules 2004;37:118.
[26] Pérez E, Benavente R, Bello A, Pereña JM, Vanderhart DL. Macromolecules 1995;28:6211.
[27] Baltá-Calleja FJ, Vonk CG. X-Ray scattering of synthetic polymers. Amsterdam: Elsevier; 1989.
[28] Ryan AJ, Stanford JL, Bras W, Nye TMW. Polymer 1997;38:759.
[29] Crist B. J Polym Sci, Part B: Polym Phys 2001;39:2454.
[30] Pérez E, Marugán MM, Vanderhart DL. Macromolecules 1993;26: 5852.
[31] Demus D, Richter L. Textures of liquid crystals. 2nd ed. Leipzig: Deutscher Verlag für Grundstoffindustries; 1980.